Low Temperature Physics/Fizika Nizkikh Temperatur, 2020, v. 46, No. 4, pp. 422–432

Microwave devices based on superconducting surface electromagnetic wave resonator

(Review Article)

V. Malyshev, G. Melkov, and O. Prokopenko

Taras Shevchenko National University of Kyiv, 64/13 Volodymyrska str., Kyiv 01601, Ukraine
E-mail: oleksandr.prokopenko@gmail.com

Received December 16, 2019, published online February 28, 2020

In this paper we present an overview of the microwave properties of a surface electromagnetic wave resonator (SEWR) made on the basis of a superconducting film, and also consider possible applications of such resonators to create various microwave devices. Features of such a SEWR are the simplicity of its design (such a resonator, in fact, can be just the superconducting film itself on a dielectric substrate); a large amplitude of microwave electromagnetic field on the surface of the resonator's superconducting film, which allows one to organize intense interaction of this field with the superconductor; the possibility of synchronous operation of integrated superconducting elements, embedded in the resonator, under the action of its microwave field. The review is based on our works published since 2000 and discusses the possible applications of superconducting SEWRs to create a new class of microwave filters, microwave signal generators and detectors, and other devices based on Josephson junctions.

Keywords: high-temperature superconductivity, surface electromagnetic wave, microwave resonator, Josephson junction.

Contents

This review paper describes microwave devices based on a novel type of microwave resonator, the surface electromagnetic wave resonator, that is suitable for the creation of high-efficiency devices that utilize arrays of Josephson junctions and relevant for the emerging field of applied superconductivity. It was purposely written for the special issue of the "Low Temperature Physics" devoted to the 80th anniversary of Professor Valerij A. Shklvoskij, who made a series of seminal theoretical contribution to the development of physics of normal and superconducting metals. The authors would like to use this opportunity to express their deep respect and gratitude to Professor Shklvoskij, and to wish him continued success in his fruitful research activity.

Introduction

Modern superconducting microwave devices (high-quality superconducting resonators, microwave receivers based on superconductor–insulator–superconductor detectors, frequency mixers, dc voltage standards, etc.) have several orders of magnitude better parameters than similar microwave devices operating at room temperatures [1–7]. Although the cooling of conventional (non-superconducting) devices to cryogenic temperatures usually improves their performance, this performance still remains worse than the performance of superconducting devices under the same conditions (at least for relatively low signal frequencies approximately less than 100 GHz) [1–7]. This advantage of superconduct-

ing devices (i.e., its high performance at microwaves) becomes most clearly seen for devices made of low-temperature superconductors that typically work at temperatures close to the liquid helium temperature (4.2 K) [2–4]. In contrast to this, devices based on high-temperature superconductors (HTSs) have a little bit worse microwave performance, but typically require only temperatures about the liquid nitrogen temperature (77 K) and rather simple and cheap cryogenic equipment for their proper operation (at least simpler and cheaper than the equipment for low-temperature devices) [1–5]. Thus, HTS devices have rather well (average) microwave performance (substantially better than for non-superconducting devices, but worse than the performance of devices based on low-temperature superconductors), but the requirements for their use are reasonable. Due to this, HTS devices usually have the best "performance/cost" value and, therefore, they are more suitable for a large number of practical applications [1–5].

To date, in fact, HTS devices can successfully compete with devices based on low-temperature superconductors mainly in the field of application of "low"- (device's quality factor, Q-factor, Q is less than 10^4) and "medium"-performance ($Q \sim 10^4$–10^6) microwave resonators and/or microwave filters [1–5,8–15]. At the same time HTS Josephson electronics is now only in the initial/middle stage of its development, while the low-temperature superconducting systems with thousands of Josephson junctions (JJs) have already been created and widely used (for example, the national voltage standard of the USA provides output dc voltage of 10 V and consists of 20260 JJs) [1–7,15–17]. The development of similar devices with hundreds and thousands of HTS JJs causes considerable complications and is only just beginning [1–5,15–19].

One should also note that recently a lot of original studies involving the novel applications of superconductors and superconductor-based resonator and circuits in the area of quantum physics research [13,14,20–22], microwave research of spin dynamics [23–25], and microwave-stimulated vortex-state response [26,27] have been reported. In addition to that promising microwave probing techniques have been developed and used for the observation and study of several physical phenomena [28–31] and then utilized for novel and relevant applications of superconductors (e.g., microwave fluxonic devices, superconducting spintronic/magnonic devices, and novel microwave metamaterials) [20,22,23,25,32–37]. We would like to especially underline here that many paper referred above are published by Prof. Valerij A. Shklovskij and his fellows, who made a crucial contribution to the development of novel vortex-based physics and applications of superconductors.

Let us consider the features of creating superconducting microwave devices with HTS JJs from the point of view of microwave technology [37]. To excite microwave signal in JJs, the junctions are usually connected to microwave transmission lines (microstrip or coplanar lines, waveguides, quasi-optical lines, etc.) or some microwave antenna (for instance, microstrip, patch or horn antennas), or they are embedded in a microwave resonator [1–5,11,15–19,37]. The last method has the following advantage — it makes possible to significantly improve the interaction of JJs with the microwave electromagnetic field. As such resonators in modern applied physics are usually used microstrip, coplanar or parallel-plate resonators consisting of two superconducting plates [1–7,11,15–22,37,38]. In either considered case, at least two superconducting films are required simultaneously, that has inevitably complicated both the resonator's fabrication and measurement processes, especially in the Ka-band (26.5–40 GHz) and at higher frequencies. Although such limitations are not very significant for microwave devices based on superconducting films [2–5,8–11, 13,14,20–25] (see also [28–37] for perspective applications of such devices), these limitations must be taken into account for devices with JJs [1–7,12–19,37,38]. Especially it is necessary to take into account the fact that the typical "volume" of the JJ is substantially smaller than the volume in which the electromagnetic field of the resonator exists. Therefore, unless special measures are taken, the interaction of the JJ with the microwave resonator field is rather weak [1–7,11,15–22,18,19,37,38].

To overcome all the mentioned limitations a new type of microwave resonator, the so-called surface electromagnetic wave resonator (SEWR), that utilizes only a single HTS film was proposed and studied in [38–48]. This resonator operates on the surface electromagnetic wave propagating along the HTS film deposited on a dielectric substrate. First investigated by A. Zommerfeld [49], nowadays, surface electromagnetic waves are widely used in integral optics and plasmonics [50–53]. Their key feature is the high electromagnetic field intensity and, as a consequence, the high electric current density near the conducting surface that, for instance, can be used for a more efficient excitation of current-driven nano-scale devices embedded in the surface and an implementation of nonlinear operation regimes of such devices [1–4,15,18,19,37–43,45–47,51–54]. Due to this feature and the simplicity of SEWR design, it can be a promising resonator to develop a variety of high-efficiency microwave HTS devices including microwave filters, signal sources and signal detectors that utilize a single JJ and arrays of JJs, signal processing devices and other devices with many JJs [37–48]. Below we analyze the performance of a SEWR and consider its typical applications in the fields of applied superconductivity and microwave technology.

1. Microwave properties of a SEWR

The simplest SEWR can be a metallic rod or plate in a free space or in a hollow rectangular waveguide [37–39]. Here we consider a more complicated and general case of SEWR, where it consists of an HTS film situated between

two different dielectric substrates [38]. One of the substrates may just be used for HTS film deposition. The whole structure is placed in a rectangular waveguide as shown schematically in Fig. 1 (note that at frequencies exceeding 50 GHz an alternative quasi-optical method of the SEWR excitation, identical to the excitation technique based on the use of dielectric prisms in plasmonics [51–53], can be utilized) [37,39].

In Fig. 1, the length (along y axis) and the width (along z axis) of the resonator are l and w, respectively. The thicknesses of the dielectric substrates are d_1 and d_2 with permittivities of ε_1 and ε_2, respectively. The HTS film thickness h is assumed to be rather small, $h << d_1, d_2, l$, and w. The dimension of the rectangular waveguide cross-sectional area is $a \times b$, and δ_1, δ_2 are the distances between the resonator and lower or upper broad waveguide walls, respectively. In general, the angle φ between the film plate and the broad waveguide walls is not equal to 90°, as it is depicted in Fig. 1.

For $d_1 = d_2 = 0$, we have the known case of the metallic plate in a waveguide or in a free space ($a = b \to \infty$) [55]. The fundamental resonance wavelength λ_r in the last case is approximately twice of the plate length l: $\lambda_r \approx 2l$ (half-wave resonator). In the other case, $d_1 = d_2 = \delta_1 = 0$, one can obtain the quarter-wave resonator having the resonance wavelength $\lambda_r \approx 4l$ [38].

The fundamental oscillation mode of the resonance structure shown in Fig. 1 has the following properties [37–48]. Its microwave currents excited by the TE_{10} wave of a rectangular waveguide flow primarily in the HTS film along the y direction. The resonance frequency is mainly determined by dimension l (along y), and the influence of dimension w (along z) on the resonance frequency is significant only when $w << l$. It was found in [38,39] that the fundamental resonance mode is formed by propagating of the quasi-uniform surface wave along y direction. Because

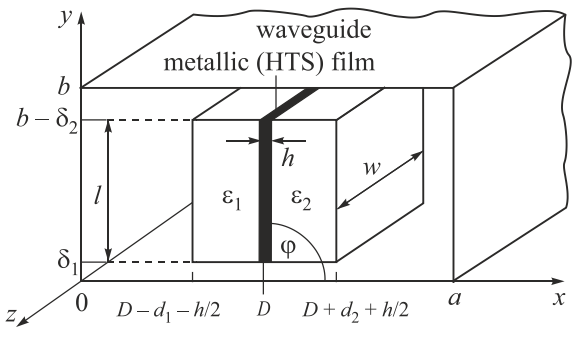

Fig. 1. Schematics of a surface electromagnetic wave resonator (SEWR) situated in a hollow rectangular waveguide with $\varphi = 90°$ (i.e., HTS film plane is perpendicular to the broad walls of the waveguide). When HTS film of the SEWR touches waveguide walls the case of quarter-wave resonator is realized, otherwise, when $\delta_1, \delta_2 \neq 0$, the resonator works as a half-wave resonator. Adopted from [38].

of close similarities in the field distributions between TE_{10} wave of a rectangular waveguide and the considered resonance mode, this last mode is easily excited by the fundamental wave TE_{10} of rectangular waveguide [37–47]. The characteristics of high microwave current density and homogeneity also make this excited mode to be very perspective for the applications in devices with JJ arrays (e.g., Josephson generator etc.) [37–47]. In addition, the fundamental mode can also be used for measuring of the complex conductivity, surface impedance, pinning and viscosity of the vortices in HTS films [37–39,41,45,46]. The ease of resonance excitation of the SEWR combines with the relatively ease of its fabrication (in fact, conventional SEWR is just an HTS film on a substrate in an empty waveguide) [37–41]. All this makes such SEWRs to be very attractive alternative for microwave devices operated in a frequency range of about 10–100 GHz.

1.1. Theory

To calculate the electromagnetic field, current distribution, frequency and quality factor Q of the resonance modes of the structure shown in Fig. 1, we used the partial region method [55]. First, the eigenwaves of the loaded infinite ($w \to \infty$) waveguide were determined. For this purpose the waveguide has been divided into four partial regions [38]:

$$\begin{aligned} &\text{I.} && 0 < x < a, && 0 < y < \delta_1, \\ &\text{II.} && 0 < x < a, && b - \delta_2 < y < b, \\ &\text{III.} && 0 < x < D, && \delta_1 < y < b - \delta_2, \\ &\text{IV.} && D < x < a, && \delta_1 < y < b - \delta_2. \end{aligned}$$

The expansion of the eigenwave electromagnetic fields in terms of the LM and LE waves (for details see [55] and references herein) of an empty waveguide was used [38]. The 20–100 lowest wave modes were considered in every region. The tangential components of electrical **E** and magnetic **H** fields were equaled on the region borders to obtain the fields and wavenumbers of the eigenwaves of the loaded infinite waveguide.

With the presence of an HTS films, it was assumed that the ratio between the tangential components of the electric E_τ and magnetic H_τ fields on each film surface $x = D \pm h/2$ is defined by the HTS film thickness and its surface impedance Z_S [2,20,21] and can be expressed as [2–4,38,56,57]

$$\frac{E_\tau}{H_\tau} = Z_S \operatorname{cth}\left(\frac{h}{\tilde{\lambda}}\right). \tag{1}$$

Here the surface impedance of the bulk HTS Z_S is defined as [2–4,56,57]

$$Z_S = R_S + jX_S = j\omega\mu_0\tilde{\lambda} = \frac{j\omega\mu_0\lambda_L}{\sqrt{1 + j\omega\mu_0\sigma_n\lambda_L^2}}, \tag{2}$$

and $\lambda_L = \lambda_L(t)$ and $t = T/T_c$ are the London penetration depth and reduced temperature, respectively. Empirically,

the temperature dependence of λ_L can be approximately described by [2–4,7,56,57]

$$\left(\frac{\lambda_L(0)}{\lambda_L(t)}\right)^2 = 1 - t^{\gamma}, \tag{3}$$

where γ is the exponential temperature parameter of superconductor [7,56,57]. For typical HTS films, $YBa_2Cu_3O_{7-\delta}$ (YBCO) films, the normal state conductivity σ_n appeared in (2) can be approximated as [57]

$$\sigma_n(t) = \sigma_n(1)\left[t^{\gamma-1} + \alpha(1-t^{\gamma})\right]. \tag{4}$$

Where $\sigma_n(1)$ is the conductivity at $T = T_c$ and α is an empirical parameter to be determined. Thus, there are five HTS film parameters (T_c, $\lambda_L(0)$, $\sigma_n(1)$, γ and α), depending on the film quality that must be determined experimentally. We also note here that the used impedance model described by Eqs. (1)–(4) is rather simple and may not account physical effects recently discovered for the vortex-state of superconductors [25–27].

Next, we analyzed the resonator characteristics by dividing the infinite loaded waveguide into three partial regions along z [38], namely,

I. $z > 0$,
II. $-w < z < 0$,
III. $z < -w$.

The tangential components of electrical and magnetic fields were equaled on the regions borders [38]. The fields in the first and the third regions were expanded by the empty waveguide wave fields. The fields in the second region were expanded by the eigenwave fields of loaded waveguide (considered above). So, the system of equations obtained from the boundary conditions for the tangential components of electrical and magnetic fields allows one to calculate the resonant frequencies of SEWR and its field distribution for different resonance modes [37,38,41,44,45]. As an example, in Fig. 2 it is shown the calculated dependence of resonant frequencies f_r of the copper plate situated in the center of a rectangular (23×10 mm) waveguide on the resonator width w. For comparison, the experimental data from [38] are also plotted in the same figure.

It can be seen that there are two groups of SEWR resonant modes: in the one group mode frequency f_r weakly depends on the resonator width w, but strongly (resonantly) depends on its length l (e.g., mode I, which is the fundamental mode of the SEWR, shown by black line and points in Fig. 2). The other group, presented by high-order modes II–IV, is characterized by a resonant dependence of f_r on SEWR width w (dashed lines and points in Fig. 2) and a weaker dependence for $f_r(l)$. The presented results demonstrate good agreement between measured and calculated data. It should be also noted that the dependence of resonance frequencies of SEWR based on a high-quality YBCO film deposited on a thin dielectric substrate with low microwave losses (too thin to have dielectric resonances) on the resonator width w is very similar to the one presented in Fig. 2 (at least for rather low temperatures $T < T_c$).

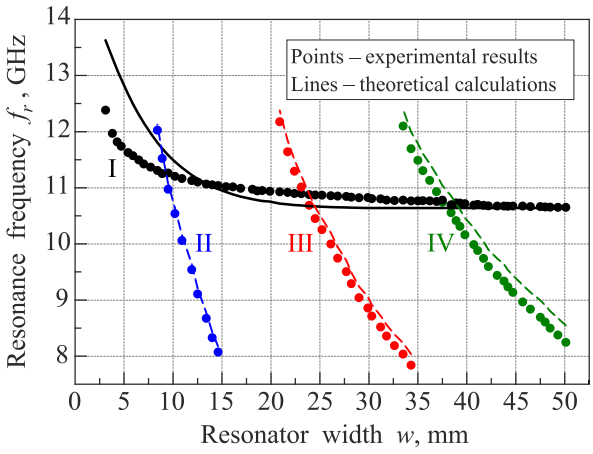

Fig. 2. Resonant frequencies of copper SEWR without dielectrics situated at the center of the standard X-band rectangular waveguide: points show the experimental data, solid lines depict the results of theoretical calculations. SEWR has the length $l = 8.8$ mm, and rotated by angle $\varphi \approx 5°$ to the waveguide broad wall. Resonant mode I is the fundamental mode of the SEWR (black line), which strongly depends on l and weakly depends on w, while modes II–IV are the high-order modes that strongly depend on the resonator width w (dashed lines). Adopted from [38].

The resonant wavelength of the fundamental mode I in Fig. 2, $\lambda_r = c / f_r$ (c is the speed of light), can be approximately represented, in the case of copper SEWR with no dielectrics, as $\lambda_r = 2(l + \Delta)$ [38,39]. Here Δ is determined by the field distribution outside the resonator. In the absence of dielectrics, there are two possible cases: $w \to 0$, $\Delta \to 0$ and $w \to \infty$, $\Delta \approx 5.5$ mm [38]. Whereas in the case of resonator with dielectric plates, the resonant wavelength becomes $\lambda_r = 2(l_\varepsilon + \Delta_\varepsilon)$ with normalized length of $l_\varepsilon = l\sqrt{\varepsilon_{\text{eff}}}$, where $\varepsilon_{\text{eff}} = \varepsilon(d_1, d_2, \varepsilon_1, \varepsilon_2)$ is the effective dielectric permittivity, $1 < \varepsilon_{\text{eff}} < \max\{\varepsilon_1, \varepsilon_2\}$; and $\Delta_\varepsilon = \Delta(l_\varepsilon, w)$, $\Delta_\varepsilon < \Delta$ [38,39].

The unloaded Q-factor of the SEWR Q_0 used in (5) was calculated by the following expression [38]:

$$\frac{1}{Q_0} = \frac{1}{Q_S} + \frac{1}{Q_d}. \tag{5}$$

Here Q_S is the Q-factor owing to the losses in 6 metallic surfaces $S = \sum_{i=1}^{6} S_i$ (i.e., in the two narrow and two broad waveguide walls and in the both HTS film surfaces), and Q_d is the Q-factor due to the losses in dielectrics. The following expressions were used for calculation of the respective Q-factors [38]:

$$\frac{1}{Q_S} = \sum_{i=1}^{6} \frac{1}{Q_{S_i}}, \quad Q_{S_i} = 2\pi f_r \frac{W}{P_{S_i}}, \quad Q_d = 2\pi f_r \frac{W}{P_d}. \tag{6}$$

The quantities appearing in the above expressions are the stored energy W, the power losses in the ith metallic surface P_{S_i}, the total power losses in the metallic/HTS surfaces $P_S = \sum_{i=1}^{6} P_{S_i}$, the power losses in dielectric substrates P_d, and the total absorbed power in the resonator $P = P_S + P_d$, respectively. They are further calculated as [38]

$$W = \int_0^a dx \int_0^b dy \int_{-\infty}^{+\infty} dz \left[\frac{\varepsilon\varepsilon_0}{4} \mathbf{E}^2 + \frac{\mu_0}{4} \mathbf{H}^2 \right], \tag{7}$$

$$P_d = \iiint_{V_d} \tan\delta \frac{\varepsilon\varepsilon_0}{4} \mathbf{E}^2 dV, \tag{8}$$

$$P_{S_i} = \frac{1}{2} \int_{S_i} [\mathbf{E}_\tau \times \mathbf{H}_\tau] d\mathbf{S}, \tag{9}$$

where V_d is the volume occupied by the dielectrics and $\tan\delta$ is the loss tangent of the dielectrics.

The simulated distribution of the linear microwave current density I, i.e., the microwave surface current (given in A/mm units) in the HTS film under the action of the absorbed power of P = 1 mW, is shown in Fig. 3. The current density values are determined by the tangential component of magnetic field H_τ on the HTS film surfaces, $H_\tau = I$. It is immediately apparent that the current distribution is far more homogeneous in the case of SEWR than in the case of a microstrip resonator [2,4,10,55]. Also as one can see from Fig. 3 the surface current distribution is symmetrical along the HTS film width w, i.e., about the center of the resonator at $z = w/2$. One further peculiarity of the microwave SEWR to be noted is the high current densities in

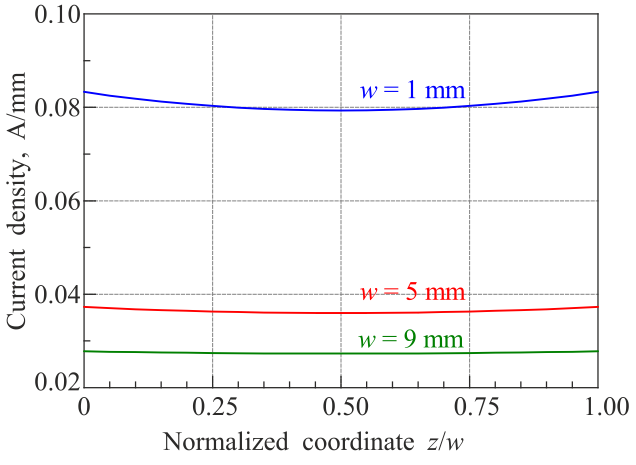

Fig. 3. The distribution of the microwave current density flow along HTS film in z direction I/I under the action of absorbed microwave power P = 1 mW. The curves are calculated for SEWR and waveguide parameters: l = 8.8 mm, ε_1 = 25, ε_2 = 9.8, $d_1 = d_2$ = 0.5 mm, R_S = 0.5 mΩ, a = 23 mm, b = 10 mm, φ = 90°, D = 11.5 mm. Adopted from [38].

the HTS films resulted from the electromagnetic field concentrating nearby conducting surfaces. Both of these unique characteristics suggest the use of HTS SEWR in the devices with JJ array [36–46]. The larger the resonator width w, the smaller the current density inhomogeneity, and hence the larger total current can flow in the structure. For instance, with w = 9 mm and l = 8.8 mm, one can obtain $I(z = w/2)/I(z = 0) = I(z = w/2)/I(z = w) = 0.993$ and the total current magnitude is 0.34 A per 1 W of the absorbed power (see Fig. 3). Thus, the fundamental mode of a SEWR (mode I in Fig. 2) having very homogeneous current distribution along the resonator size w (achieved for the resonator of sufficiently large width w) is quite convenient for the creation of HTS devices with many JJs, because in such a system all JJs can be biased by almost the same ac currents. Moreover, due to the specific features of surface electromagnetic waves [37,38,50–53] and interaction between HTS film and JJs with the resonator field, all junctions could operate in the same excitation conditions despite the fact that they could have substantially different electrical and/or microwave characteristics. Consequently, the SEWR plays a role of natural microwave system able to provide an efficient synchronization of JJs with substantially different electrical and/or microwave parameters dependent on the quality level of used junction fabrication technology [37–47].

1.2. Experimental results

We have experimentally investigated SEWRs made from YBCO films grown on single crystalline $LaAlO_3$ substrates [37–41,45]. The dimensions of the substrates are l = 10 mm, w = 5 mm or w = 10 mm, and its thickness is d_1 = 0.5 mm (see Fig. 1). The YBCO films were about 0.4 μm in thickness. The $LaAlO_3$ substrate, having the permeability of ε_1 = 25, was serving as one of the dielectrics in the SEWR. The temperature dependence coefficient of ε_1 was less than $1.6 \cdot 10^{-3}$ over the temperature range from 50 to 100 K, as it was confirmed by measurements for the SEWR copper film / $LaAlO_3$ substrate. The second dielectric was sapphire with permittivity ε_2 = 9.8 and thickness d_2 = 0.5 mm or d_2 = 1.0 mm. Measurements were also performed without the second dielectric (i.e., d_2 = 0 and ε_2 = 1) [37–41,45].

Below we report the temperature dependences of the fundamental mode frequency f_r and the unloaded quality factor Q_0 of the HTS SEWR. Both f_r and Q_0 were measured at a fixed temperature by the standing wave coefficient technique [58]. To increase the measurement precision, f_r was measured using match-terminated waveguide. To obtain such purpose, the matching load was located beyond the resonator (at $z < -w$, see Fig. 1). Furthermore, in order to optimize the coupling between the resonator and the waveguide, the angle φ between film plane and broad walls of waveguide (see Fig. 1) has to be small, practically $\varphi \le 10°$ [38]. Indeed, it was evident that when

the above conditions were fulfilled, the resonance curve was extremely narrow and sufficiently high. To measure Q_0 the critical coupling was fixed with a short-circuit plunger beyond the resonator in place of matched load [58]. This method is unsuitable for frequency measurements owing to frequency pulling. The measurement precision of Q_0 and f_r was better than 10% and 20 MHz, respectively [37–48].

The typical temperature dependences $f_r(T)$ and $Q_0(T)$ measured for the HTS SEWR with chosen parameters situated in a standard X-band rectangular waveguide are shown by points in Figs. 4 and 5, respectively [38]. For comparison, the theoretical curves of $f_r(T)$ and $Q_0(T)$ calculated by using the above described model (see Sec. 1.1) and appropriate parameters are displayed by lines in the same figures. The theoretical curves in Figs. 4, 5 were calculated with an account of the following chosen system parameters: the HTS film critical temperature T_c, London penetration depth $\lambda_L(0)$ at 0 K, normal conductivity $\sigma_n(1)$ at $T = T_c$, exponent γ and residual resistance rate α. The values of T_c of the YBCO films were determined by the standard four-probe transport measurements performed on control samples made at the same deposition run [38]. The $\lambda_L(0)$ value was inferred from previous stripline resonator measurement [59]. The remaining parameters were determined by measuring the surface resistance R_S. These measurements were made at a frequency of 67 GHz by replacing the copper end face of a cylindrical cavity resonator with H_{011} mode oscillation by an HTS film [60]. By adjusting $\sigma_n(1)$, γ, and α for each film, we obtained the best fit between the theoretical expressions (1)–(4) and the experimental data.

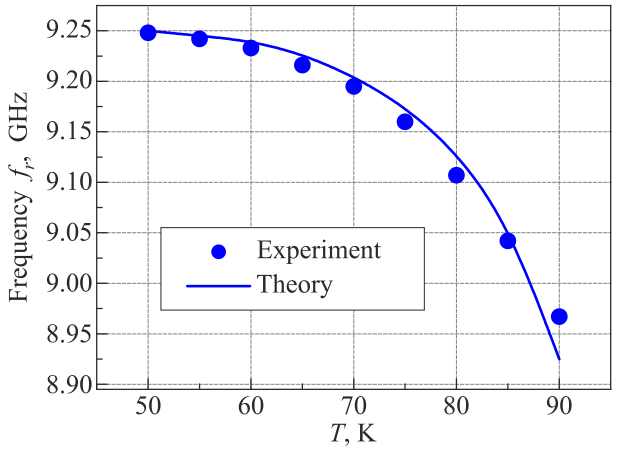

Fig. 4. Measured (points) and simulated (line) dependences of resonant frequency f_r of the HTS surface wave resonator fundamental mode on temperature T for the case: $l = 10$ mm, $w = 5$ mm, $d_1 = d_2 = 0.5$ mm, $h = 0.4$ μm, $\varepsilon_1 = 25$, $\varepsilon_2 = 9.8$, $\varphi = 11°$, $T_c = 91$ K, $\lambda_L(0) = 0.2$ μm, $\sigma_n(1) = 1.5 \cdot 10^6\ \Omega^{-1} \cdot \mathrm{m}^{-1}$, $\gamma = 4$, $\alpha = 15$. The observed temperature dependence of the resonance frequency of HTS SEWR is caused by the temperature dependence of HTS film impedance (see Eq. (1)), which, in turn, does influence on the fundamental mode's electromagnetic energy distribution near the surface of HTS film. Adopted from [38].

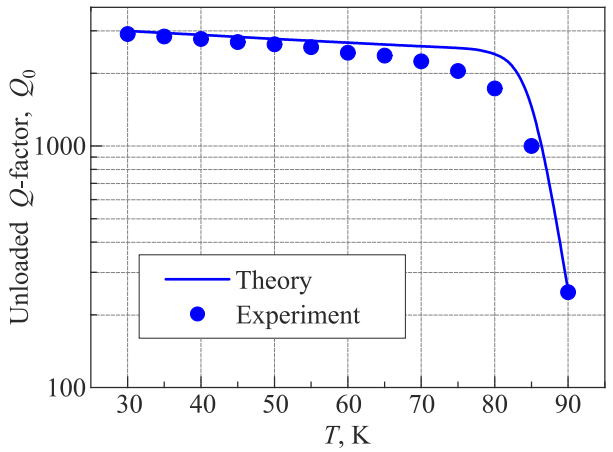

Fig. 5. Measured (points) and simulated (line) temperature dependences of Q-factor of the HTS SEWR. The fitting parameters are the same as those used for Fig. 4. Adopted from [38].

Figure 6 shows the results of fitting the simulated curve $R_S(T)$ to the experimental data shown in Figs. 4, 5 with $T_c = 91$ K, $\lambda_L(0) = 0.2$ μm, $\sigma_n(1) = 1.5 \cdot 10^6\ \Omega^{-1}\mathrm{m}^{-1}$, $\gamma = 4$, and $\alpha = 15$, respectively [38]. The general agreement between theory and experiment is indicative of the viability of the used technique.

It should be noted that the shift of the resonant frequency f_r, caused by the changes of surface reactance X_S, can reach several hundreds of MHz over a temperature span of 40 K (Fig. 4). The presented technique, thus, provides a useful and convenient alternative for studying the microwave properties of HTS films [38]. Also later, up to ~ 600 MHz frequency shift has been obtained on films having better R_S: $R_S(70\,\mathrm{K}) = 21$ mΩ as compared to $R_S(70\,\mathrm{K}) = 29$ mΩ for films shown in Figs. 4–6.

The quality factor $Q_0(T)$ of the HTS SEWR (Fig. 5) at $T < 70$ K is determined predominantly by losses in the copper walls of the waveguide (because the electromagnetic field

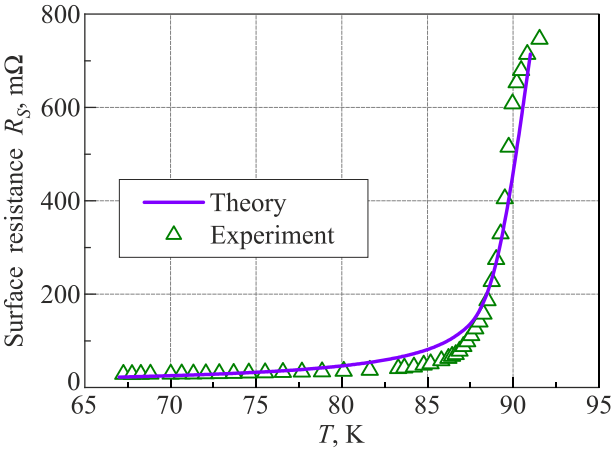

Fig. 6. Measured (points) and simulated (line) temperature dependences of the surface resistance of the SEWR based on YBCO film. The fitting parameters are the same as those used in Figs. 4 and 5. Adopted from [38].

of surface microwave oscillations exist rather far beyond geometrical borders of the resonator). Higher Q-factors are expected by using thicker dielectric plates with higher dielectric permittivity and by placing resonator into an oversized waveguide [38]. The maximum theoretical Q-factor value for an HTS SEWR with $R_S = 0.5$ mΩ placed in standard rectangular waveguide is equal to $Q_0 \sim 8 \cdot 10^4$ [38]. An alternative promising technique for the increase of the resonator's Q-factor, which implies SEWR situation in a center of a below-cutoff waveguide, was proposed, tested and verified in [44–47].

2. Microwave devices based on HTS SEWR with JJ array

2.1. Performance of HTS JJs embedded in a SEWR

It is well known that the embedding of nonlinear elements like JJs in a resonator may cause the distortion of the resonance mode field distribution and decrease of the resonator's Q-factor [1–7,11–15,19,37–47]. At the same time these changes also affect the performance of nonlinear elements embedded in a resonator. Because of that the problem of choosing the optimal embedding topology for JJs is important. The main aim of such an optimal topology is to ensure the high coupling of the SEWR with nonlinear elements (Josephson junctions) and minimize the losses of SEWR performance (reduction of its Q-factor and frequency stability, worsening the ability to synchronize JJs under the action of a field of the surface electromagnetic wave, discussed in Sec. 2, etc.).

In our studies we used bicrystal HTS JJs as nonlinear elements integrated in the SEWR and considered the cases, when the number of junctions varied from 1 to 450 [37, 40–47]. We analyzed the efficiency of several possible topologies for embedding HTS JJs in a SEWR and chose the topology that can be referred as the series-shifted parallel [1–7,15–18,40–43,45–47]; it is schematically shown in Fig. 7 (all sizes in the figure are in μm). In this case HTS YBCO film is grown on the top of a dielectric substrate with the bicrystal grain boundary at which JJs can form. In typical experimental situation the length of bicrystal boundary is equal or comparable to the resonator width w, which is equal to the width of the substrate, therefore, in the case of continuous HTS film a very wide (with width ~ w) single JJ or several wide JJs can form at the boundary. To substantially reduce the width of JJs (that, usually, due to the reduction of junction capacitance leads to the improvement of their characteristics [1–7,16–19]), we made slits in the continuous HTS film by mechanically removing some parts of the film or by using the lithographic patterning technique (see Fig. 7, where black areas correspond to the remaining parts of the YBCO film) [40–43,45–47]. Due to these modifications of HTS film, a set of rather narrow JJs of ~ 4 μm width were formed in the film at the region close to the bicrystal boundary (see Fig. 7) [40–43,45–47]. In such a device topology, JJs are series dc connected (dc current flows in the parts of HTS film shown by black areas in Fig. 7 from the left-top corner of the sample to its right-bottom corner crossing each JJ only once) and parallel connected at a microwave current (this current flows in the direction perpendicular to the bicrystal boundary) [40–43,45–47]. Note that the structures like one shown in Fig. 7 (or even smaller, if needed) can now be fabricated by focused ion beam induced deposition, without lithographic patterning, and even extended into the third dimension (e.g., see [1,2,15,18,61]).

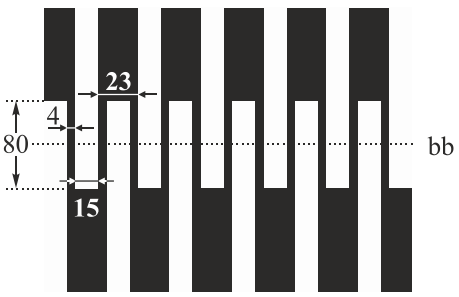

Fig. 7. Topology of HTS film in the SEWR (black areas correspond to the HTS). All sizes are in micrometers. bb shows the bicrystal grain boundary.

We have shown theoretically and experimentally [41–43,45–47] that the Q-factor of the SEWR with topology is decreased, when the number of JJs (or slits in HTS film) is increased. The lower limit of Q-factor decreasing is near 50% of initial Q-factor of the SEWR without topology when the number of JJs is below 10^3. Therefore, formally one can use SEWR-based systems with an array of about several hundreds of junctions or less, that is the necessary condition for the creation of voltage standards and Josephson generators [41–43,45–47].

It was also carried out the measurement of current-voltage curve (CVC) of a single junction and an array of JJs. In Fig. 8 it is shown CVC for the array with 6 HTS JJs embedded in the SEWR [41,45]. It can be clearly seen that all junctions work synchronously, so the summary current steps I_n appear on the CVC (n is the step number). In Fig. 9 it is also shown the dependence of the normalized current steps I_n / I_c for the first four steps (n = 0, 1, 2, 3, I_c is the JJ critical current) on the external microwave power P for the array with 6 junctions proving the previous thesis [41,45]. It is necessary to pay attention to the fact that both dependences are smooth and their behavior is very similar to the behavior of an ideal JJ, when current step amplitude is determined by Bessel's functions [1–7,15,18,19].

Note that such experiments were performed for arrays with different number of junctions: 4 [40], 6 [41,45], 180 [46,47], 207 [43], and up to 450 [45] junctions. For all used samples it was observed the junction synchronization effect, and in the case of 450 junctions the current steps were obtained at ~10, 20, and ~30 mV [45].

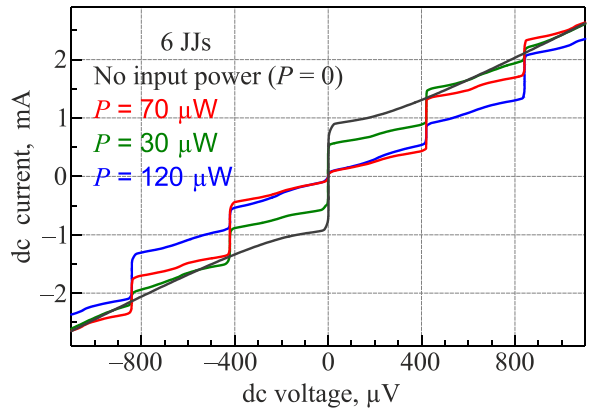

Fig. 8. (Color online) Current-voltage curves for JJ array with 6 junctions embedded in the SEWR measured for different incident microwave power P. Adopted from [41,45–47].

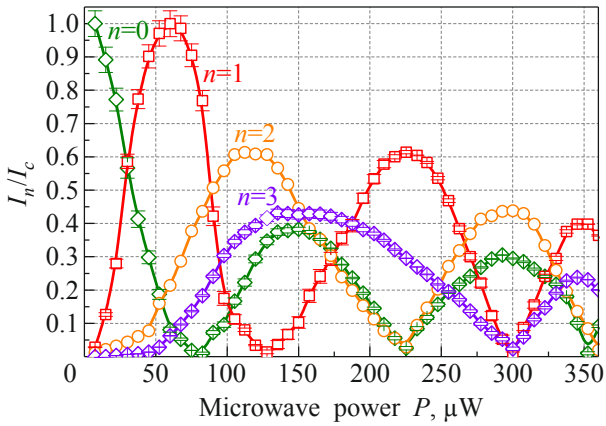

Fig. 9. Normalized dependences of summary current steps I_n / I_c on external microwave power P for an array with 6 JJs embedded in the SEWR (I_c is the junction critical current, n is the step number). Adopted from [41,45–47].

2.2. Signal generator and detector based on SEWR with embedded JJ array

We also investigated the microwave detectors based on HTS JJ arrays. For the detector based on arrays consist of 180 JJs [46,47] and 450 JJs [45], the measured ampere-watt sensitivity was about 0.1 A/W and dynamics range ~ 10^2 dB at 77 K.

The observed synchronization effect for JJs under the action of an external microwave irradiation (i.e., JJs dc response to a microwave signal) [45] (see also Fig. 9) allows one to suggest that the Josephson generation (junctions' microwave response to a dc signal) of an array of HTS JJs in the SEWR will be also coherent. It permits to create microwave tunable generators in a wide frequency range including sub-millimeter band, where the electromagnetic generation problem has a high priority nowadays.

We investigated the generation in an array of JJs embedded in the SEWR to prove the possibility of creation of Josephson generator [41–43]. The quarter-wave resonator was fabricated on yttrium-stabilized zirconium substrate with a single bicrystal grain boundary, and epitaxial YBCO HTS film was deposited over it. Bicrystal grain boundary with misorientation angle of 19° was located in the center of the SEWR. There were 450 shunted JJs in the HTS film. Some part of them took part in the Josephson generation [41–43]. The topology of JJ array was similar to those, shown in Fig. 7.

In Fig. 10 there are shown the dependences of Josephson radiation power and their frequency on the total dc voltage applied to the JJ array. One can see that the intrinsic electromagnetic radiation of several hundreds of nW exists. As it is expected, the Josephson radiation frequency f depends on the total voltage V, but the frequency/voltage ratio was approximately one-half of the theoretical value [1–7,41–43,45]. We think this was happen due to the effect of frequency pulling by the resonator and due to the variation of number of synchronously working junctions (not all junction in the array may work synchronously), when the voltage is changing (this quantity is mainly increased with the voltage). Spectrum of Josephson generation at the generation zones is determined mainly by the voltage bias for summary current steps and was changed from some tens of MHz to hundreds of kHz [41–43,45]. There was observed a small increase in power generation (up to the factor of 1.5

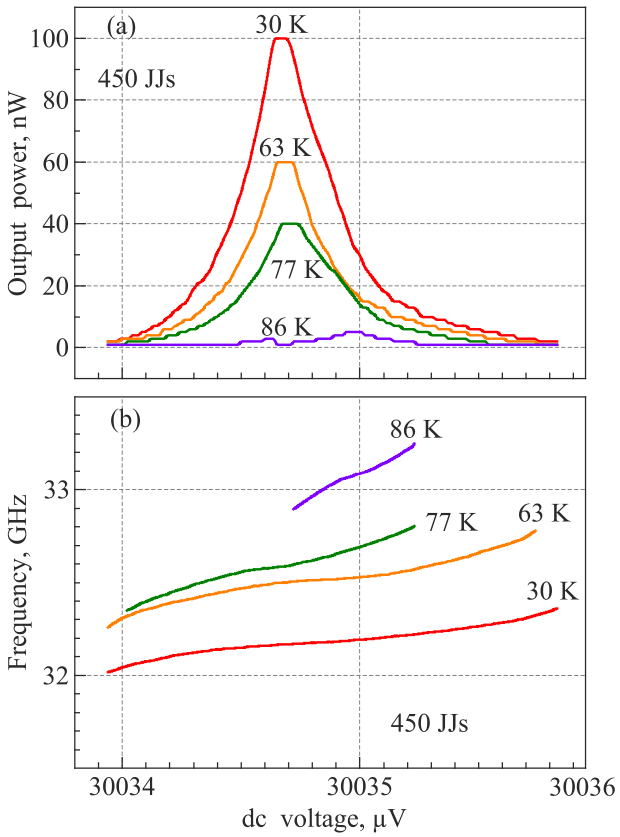

Fig. 10. Dependences of an output power (a) and generation frequency (b) on applied dc voltage at various temperatures T for a JJ array with 450 junctions embedded in the SEWR. Adopted from [42,43,45].

at $T = 30$ K) and decrease of the generation zone (along voltage axis) when the temperature is falling down [41–43,45]. The change of SEWR Q-factor with temperature (see Fig. 5) can explain this effect.

The obtained results evidently show that the SEWR can be successfully used to create practical microwave devices with JJ arrays (e.g., voltage standards, signal sources and detectors, etc.) consisting up to 450 junctions. However, for such devices based on YBCO films with JJ arrays, the degradation of the SEWR performance, and hence the performance of the entire device, becomes observable for the number of junctions $N \geq 200$. This limitation is crucial enough, because in modern superconducting devices thousands and tens of thousands of JJs are frequently used [1–7, 15–19,62]. Another principal limitation of the considered system is the placement of SEWR inside a rectangular waveguide for proper resonator excitation. Obviously, this makes impossible the full use of such systems in modern superconducting micro- and nanoelectronics, while the known systems based on planar (usually, microstrip or coplanar) resonators even with smaller number of embedded JJs have clear advantages for micro- and nano-scale applications [63–66]. Nevertheless, the discussed SEWRs based on HTS films with JJ arrays can be used for the creation and development of "average-quality" superconducting devices with ~ 500 JJs or less providing an output microwave power of ~ 100 nW (regime of the Josephson generation), output dc voltage of ~ 30 mV (dc votage standard regime) and a rather efficient signal detection (detector ampere-watt sensitivity is about 0.1 A/W and its dynamic range of powers ~ 100 dB) in X- and Ka-bands. Also such SEWRs can be used for the study of microwave properties of novel types of JJs, like Mo–Re junctions with very high values of characteristic voltage [67,68], as well as the study of synchronization phenomena in strongly nonlinear nanoscale systems (like JJs) [37,69] embedded in a surface of HTS film.

Conclusions

We have shown that a surface electromagnetic wave resonator (SEWR) based on high-temperature superconductor (HTS) films have a number of advantages compared to planar and cavity resonators: the simplicity of SEWR design (it can be an HTS film itself on a dielectric substrate), and a strong interaction between the resonator electromagnetic field and an HTS film providing the forced synchronization of Josephson junctions (JJs) created in the HTS film by a microwave field of the resonator. Such a superconducting SEWR with 1–450 embedded JJs can be used for the creation of "average performance" microwave signal generators (output power ~ 100 nW), detectors (sensitivity ~ 0.1 A/W, dynamical range of powers ~ 100 dB), and voltage standards with output dc voltage of ~ 30 mV operating in the X- and Ka-bands. Although SEWR is not very suitable for micro- and nano-scale applications, nevertheless it can be successfully used for the study of novel types of JJs and their synchronization phenomena under the action of microwave electromagnetic field.

Acknowledgment

This work was supported in part by the grants Nos. 18BF052-01M and 19BF052-01 from the Ministry of Education and Science of Ukraine and grant No. 1F from the National Academy of Sciences of Ukraine.

1. *Fundamentals and Frontiers of the Josephson Effect*, F. Tafuri (ed.), Springer, New York (2019).
2. H. Liu, B. Ren, X. Guan, P. Wen, and T. Zuo, *High-Temperature Superconducting Microwave Circuits and Applications*, Springer, Singapore (2019).
3. *Applied Superconductivity*: *Handbook on Devices and Applications*, P. Seidel (ed.), Wiley-VCH, New Jersey (2015).
4. S.T. Ruggiero, *Superconducting Devices*, Elsevier, Amsterdam (2013).
5. N. Newman and W.G. Lyons, *J. Supercond.* **6**, 119 (1993).
6. A. Barone and G. Paternò, *Physics and Applications of the Josephson Effect*, Wiley, New York (1982).
7. T. Van Duzer and C.W. Turner, *Principles of Superconductive Devices and Circuits*, Elsevier, Amsterdam (1981).
8. J. Sheng-Hong, E.P. McEarlean, and B.M. Karyamapudi, *IEEE Transactions on Microwave Theory and Technique* **53**, 2808 (2005).
9. M.J. Lancaster, *Passive Microwave Device Applications of High-Temperature Superconductors*, Cambridge University Press, Cambridge (2006).
10. J.-S. Hong, *Microstrip Filters for RF/Microwave Applications*, 2nd ed., Wiley, New York (2011).
11. J. Zmuidzinas, *Ann. Rev. Cond. Matter Phys.* **3**, 169 (2012).
12. G. Wendin, *Rep. Progr. Phys.* **80**, 106001 (2017).
13. J.K. Moqadam, M.C. de Oliveira, and R. Portugal, *Phys. Rev. B* **95**, 144506 (2017).
14. L. Sun, N. Cherpak, A. Barannik, Y.-S. He, V. Glamazdin, X. Zhang, J. Wang, and V. Zolotaryov, *IEEE Transactions on Applied Superconductivity* **27**, 1501304 (2017).
15. *Nonlinear Superconductive Electronics and Josephson Devices*, G. Costabile, S. Pagano, S. Pedersen, and M. Russo (eds.), Springer, Berlin (2012).
16. C.A. Hamilton, *Rev. Sci. Instrum.* **71**, 3611 (2000).
17. M. Darula, T. Doderer, and S. Beuven, *Supercond. Sci. Techn.* **12**, 1 (1999).
18. *Superconductors at the Nanoscale*: *From Basic Research to Applications*, R. Wördenweber, V. Moshchalkov, S. Bending, and F. Tafuri (eds.), Walter de Gruyter GmbH & Co KG, Berlin (2017).
19. *Fundamentals of Superconducting*, A. Sidorenko (ed.), Nanoelectronics, Springer, Berlin (2011).
20. H. Huebl, C.W. Zollitsch, J. Lotze, F. Hocke, M. Greifenstein, A. Marx, R. Gross, and S.T.B. Goennenwein, *Phys. Rev. Lett.* **111**, 127003 (2013).
21. Y. Tabuchi, S. Ishino, T. Ishikawa, R. Yamazaki, K. Usami, and Y. Nakamura, *Phys. Rev. Lett.* **113**, 083603 (2014).

22. R.G.E. Morris, A.F. van Loo, S. Kosen, and A.D. Karenowska, *Sci. Rep.* **7**, 11511 (2017).
23. I.A. Golovchanskiy, N.N. Abramov, V.S. Stolyarov, V.V. Bolginov, V.V. Ryazanov, A.A. Golubov, and A.V. Ustinov, *Adv. Funct. Mater.* **28**, 1802375 (2018).
24. K.-R. Jeon, C. Ciccarelli, A.J. Ferguson, H. Kurebayashi, L.F. Cohen, X. Montiel, M. Eschrig, J.W.A. Robinson, and M.G. Blamire, *Nature Mater.* **17**, 499 (2018).
25. O.V. Dobrovolskiy, R. Sachser, T. Brächer, T. Böttcher, V.V. Kruglyak, R.V. Vovk, V.A. Shklovskij, M. Huth, B. Hillebrands, and A.V. Chumak, *Nature Phys.* **15**, 477 (2019).
26. A. Lara, F.G. Aliev, A.V. Silhanek, and V.V. Moshchalkov, *Sci. Rep.* **5**, 9187 (2015).
27. O.V. Dobrovolskiy, R. Sachser, V.M. Bevz, A. Lara, F.G. Aliev, V.A. Shklovskij, A.I. Bezuglyj, R.V. Vovk, and M. Huth, *Phys. Status Solidi (RRL)* **13**, 1800223 (2019).
28. P.-de-J. Cuadra-Solís, A. García-Santiago, J. Manel Hernandez, J. Tejada, J. Vanacken, and V.V. Moshchalkov, *Phys. Rev. B* **89**, 054517 (2014).
29. S. Lösch, A. Alfonsov, O.V. Dobrovolskiy, R. Keil, V. Engemaier, S. Baunack, G. Li, O.G. Schmidt, and D. Bürger, *ACS Nano* **13**, 2948 (2019).
30. L. Embon, Y. Anahory, Ž.L. Jelić, E.O. Lachman, Y. Myasoedov, M.E. Huber, G.P. Mikitik, A.V. Silhanek, M.V. Milošević, A. Gurevich, and E. Zeldov, *Nature Commun.* **8**, 85 (2017.
31. O.V. Dobrovolskiy, V.M. Bevz, M.Yu. Mikhailov, O.I. Yuzephovich, V.A. Shklovskij, R.V. Vovk, M.I. Tsindlekht, R. Sachser, and M. Huth, *Nature Commun.* **9**, 4927 (2018).
32. O.V. Dobrovolskiy, R. Sachser, M. Huth, V.A. Shklovskij, R.V. Vovk, V.M. Bevz, and M.I. Tsindlekht, *Appl. Phys. Lett.* **112**, 152601 (2018).
33. N.T. Cherpak, A.A. Lavrinovich, A.I. Gubin, and S.A. Vitusevich, *Appl. Phys. Lett.* **105**, 022601 (2014).
34. O.V. Dobrovolskiy and M. Huth, *Appl. Phys. Lett.* **106**, 142601 (2015).
35. V.K. Vlasko-Vlasov, F. Colauto, T. Benseman, D. Rosenmann, and W.-K. Kwok, *Sci. Rep.* **6**, 36847 (2016).
36. O.V. Dobrovolskiy, M. Huth, and V.A. Shklovskij, *Appl. Phys. Lett.* **107**, 162603 (2015).
37. O.V. Prokopenko, D.A. Bozhko, V.S. Tyberkevych, A.V. Chumak, V.I. Vasyuchka, A.A. Serga, O. Dzyapko, R.V. Verba, A.V. Talalaevskij, D.V. Slobodianiuk, Yu.V. Kobljanskyj, V.A. Moiseienko, S.V. Sholom, and V.Yu. Malyshev, *Ukr. J. Phys.* **64**, 888 (2019).
38. G.A. Melkov, Y.V. Egorov, O.M. Ivanyuta, V.Y. Malyshev, H.K. Zeng, Kh. Wu, and J.Y. Juang, *J. Supercond.* **13**, 95 (2000).
39. G.A. Melkov and Yu.V. Egorov, *Fiz. Nizk. Temp*. **26**, 148 (2000) [*Low Temp. Phys.* **26**, 108 (2000)].
40. A.M. Klushin, E. Goldobin, G.A. Melkov, O.M. Ivanjuta, Y.V. Eghorov, K. Numssen, and M. Siegel, *IEEE Transactions on Applied Superconductivity* **11**, 944 (2001).
41. G.A. Melkov, O.M. Ivanyuta, O.V. Prokopenko, V.M. Raksha, A.M. Klushin, and M. Siegel, *Embedding of Josephson Junctions in the Surface Wave Resonator in the Ka-band*, *Proceedings of the Fourth International Kharkov Symposium on Physics and Engineering of Millimeter and Sub-Millimeter Waves* (*MSMW'2001*, *4–9 June 2001*, *Kharkov*, *Ukraine*) **1**, 363 (2001).
42. A.M. Klushin, O.M. Ivanyuta, K. Numssen, G.A. Melkov, and M. Siegel, *Physica C*: *Superconductivity* **372–376**, 305 (2002).
43. G.A. Melkov, Y.V. Egorov, A.N. Ivanyuta, A.M. Klushin, M. Siegel, and R. Semerad, *Izvestiya Vysshikh Uchebnykh Zavedenij. Radioelektronika* **45**, 38 (2002) (in Russian).
44. G.A. Melkov, A.V. Prokopenko, and V.N. Raksha, *Radioelectronics and Communications Systems* **47**, 20 (2004).
45. G.A. Melkov, A.M. Klushin, O.D. Poustylnik, O.V. Prokopenko, and V.M. Raksha, *Irradiation of HTS Josephson Junctions with the Surface Wave Resonator*, *Proceedings of the Fifth International Kharkov Symposium on Physics and Engineering of Millimeter and Sub-Millimeter Waves* (*MSMW'2004*, *21–26 June 2004*, *Kharkov*, *Ukraine*) **2**, 128 (2004).
46. O.M. Ivanyuta, O.V. Prokopenko, Ya.I. Kishenko, V.M. Raksha, and A.M. Klushin, *J. Low Temp. Phys.* **139**, 97 (2005).
47. O.M. Ivanyuta, O.V. Prokopenko, V.M. Raksha, and A.M. Klushin, *Phys. Status Solidi C* **2**, 1688 (2005).
48. G.A. Melkov, O.V. Prokopenko, and V.M. Raksha, *Microwave HTS Filter Based on Coupled Surface Wave Resonators*, *Proceedings of the Tenth International Kharkov Symposium on Physics and Engineering of Microwaves*, *Millimeter*, *and Sub-Millimeter Waves* (*MSMW'2007*, *25–30 June 2007*, *Kharkov*, *Ukraine*) **1**, 401 (2007).
49. A. Sommerfeld, *Ann. Phys. Chem.* **303**, 233 (1899).
50. J.A. Polo, Jr., and A. Lakhtakia, *Laser & Photonics Rev.* **5**, 234 (2011).
51. S.A. Maier, *Plasmonics*: *Fundamentals and Applications*, Springer, New York (2007).
52. *Plasmonics*: *From Basics to Advanced Topics*, S. Enoch and N. Bonod (eds.), Springer, Berlin (2012).
53. F. Yang and Y. Rahmat-Samii, *Surface Electromagnetics*: *With Applications in Antenna*, Microwave, and Optical Engineering, Cambridge University Press, Cambridge (2019).
54. *Nanoscience and Engineering in Superconductivity*, V. Moshchalkov, R. Woerdenweber, and W. Lang (eds.), Springer, Berlin (2010).
55. L. Lewin, *Advanced Theory of Waveguides*, Butterworth and Co Ltd., London (1975).
56. M.W. Coffey and J.R. Clem, *Phys. Rev. B* **17**, 9872 (1992).
57. O.G. Vendik, I.B. Vendik, and D.I. Kaparkov, *IEEE Transactions on Microwave Theory and Techniques* **46**, 469 (1998).
58. E.L. Ginston, *Microwave Measurements*, McGraw-Hill Book Company, Inc., New York (1957).
59. M.C. Hsieh, T.Y. Tseng, S.M. Wei, C.M. Fu, K.H. Wu, J.Y. Juang, T.M. Uen, and Y.S. Gou, *Chinese J. Phys.* **34**, 606 (1996).
60. G.A. Melkov, A.L. Kasatkin, and V.Y. Malyshev, *Fiz. Nizk. Temp.* **20**, 868 (1994) [*Low Temp. Phys*. **20**, 680 (1994)].
61. F. Porrati, S. Barth, R. Sachser, O.V. Dobrovolskiy, A. Seybert, A.S. Frangakis, and M. Huth, *ACS Nano* **13**, 6287 (2019).

62. R. Behr, O. Kieler, J. Kohlmann, F. Müller, and L. Palafox, *Measurement Science and Technology* **23**, 124002 (2012).
63. N.A. Masluk, I.M. Pop, A. Kamal, Z.K. Minev, and M.H. Devoret, *Phys. Rev. Lett.* **109**, 137002 (2012).
64. J. Hassel, H. Seppä, L. Grönberg, and I. Suni, *Rev. Sci. Instrum.* **74**, 3510 (2003).
65. P. Barbara, A.B. Cawthorne, S.V. Shitov, and C.J. Lobb, *Phys. Rev. Lett.* **82**, 1963 (1999).
66. A. M. Klushin, M. He, S.L. Yan, and N. Klein, *Appl. Phys. Lett.* **89**, 232505 (2006).
67. V.E. Shaternik, A.P. Shapovalov, V.P. Bloshchit-Skiy, D.S. Zhabko, E.V. Kudrya, A.V. Prokopenko, and R.A. Kuznetsov, *Metallofizika i Noveishie Tekhnologii* **34**, 275 (2012).
68. V. Shaternik, M. Belogolovskii, T. Prikhna, A. Shapovalov, O. Prokopenko, D. Jabko, O. Kudrja, O. Suvorov, and V. Noskov, *Physics Procedia* **36**, 94 (2012).
69. O.R. Sulymenko and O.V. Prokopenko, *Microwave Phase-Locking of Weakly Coupled Spin-Torque Nano-Oscillators: The Case of Global Coupling*, in book: *Nanophysics, Nanomaterials, Interface Studies, and Applications. Springer Proceedings in Physics*, O. Fesenko and L. Yatsenko (eds.), Springer-Verlag, Berlin (2017), Vol. 195.

НВЧ пристрої на основі надпровідного резонатора поверхневої електромагнітної хвилі (Огляд)

В. Малишев, Г. Мелков, О. Прокопенко

Представлено огляд мікрохвильових властивостей резонатора поверхневої електромагнітної хвилі (РПЕХ), виготовленого на базі плівки надпровідника, а також розглянуто можливі застосування таких резонаторів для створення різних мікрохвильових пристроїв. Особливостями такого РПЕХ є простота конструкції (таким резонатором фактично є сама надпровідна плівка на діелектричній підкладці); велика амплітуда електромагнітного мікрохвильового поля на поверхні надпровідника, що дозволяє організувати інтенсивну взаємодію поля з надпровідником; можливість синхронної роботи інтегральних надпровідних елементів, інтегрованих в резонатор, під дією його мікрохвильового поля. В даному огляді, грунтуючись на наших роботах, опублікованих починаючи з 2000 року, розглядаються можливі застосування надпровідних РПЕХ для створення нового класу мікрохвильових фільтрів, генераторів та детекторів мікрохвильових сигналів, а також інших пристроїв на основі джозефсонівських контактів.

Ключові слова: високотемпературна надпровідність, поверхнева електромагнітна хвиля, мікрохвильовий резонатор, джозефсонівський контакт.

СВЧ приборы на основе сверхпроводящего резонатора поверхностной электромагнитной волны (Обзор)

В. Малышев, Г. Мелков, А. Прокопенко

Представлен обзор микроволновых свойств резонатора поверхностной электромагнитной волны (РПЭВ), изготовленного на базе пленки сверхпроводника, а также рассмотрены возможные применения таких резонаторов для создания различных микроволновых устройств. Особенностями такого РПЭВ являются простота конструкции (таким резонатором фактически является сама сверхпроводящая пленка на диэлектрической подложке); большая амплитуда электромагнитного микроволнового поля на поверхности сверхпроводника, что позволяет организовать интенсивное взаимодействие поля со сверхпроводником; возможность синхронной работы интегральных сверхпроводящих элементов, интегрированных в резонатор, под действием его микроволнового поля. В данном обзоре, основываясь на наших работах, опубликованных начиная с 2000 года, рассматриваются возможные применения сверхпроводящих РПЭВ для создания нового класса микроволновых фильтров, генераторов и детекторов микроволновых сигналов, а также других устройств на основе джозефсоновских контактов.

Ключевые слова: высокотемпературная сверхпроводимость, поверхностная электромагнитная волна, микроволновый резонатор, джозефсоновский контакт.